Structural Studies of Cytochrome b_5: Complete Sequence-Specific Resonance Assignments for the Trypsin-Solubilized Microsomal Ferrocytochrome b_5 Obtained from Pig and Calf†

R. D. Guiles,‡,§ John Altman,§ Irwin D. Kuntz,§ and Lucy Waskell*,‡

Department of Pharmaceutical Chemistry, Department of Anesthesia, and Liver Center, University of California, San Francisco, California 94143, and Anesthesiology Service, Veterans Administration Medical Center, San Francisco, California 94121

Received June 14, 1989; Revised Manuscript Received October 2, 1989

ABSTRACT: We report complete sequence-specific proton resonance assignments for the trypsin-solubilized microsomal ferrocytochrome b_5 obtained from calf liver. In addition, sequence-specific resonance assignments for the main-chain amino acid protons (i.e., C^{α}, C^{β}, and amide protons) are also reported for the porcine cytochrome b_5. Assignment of the majority of the main-chain resonances was rapidly accomplished by automated procedures that used COSY and HOHAHA peak coordinates as input. Long side chain amino acid spin system identification was facilitated by long-range coherence-transfer experiments (HOHAHA). Problems with resonance overlap were resolved by examining differences between the two-dimensional 500-MHz NMR spectra of rabbit, pig, and calf proteins and by examining the temperature-dependent variation of amide proton resonances. Calculations of the aromatic ring-current shifts for protons that the X-ray crystal structure indicated were proximal to aromatic residues were found to be useful in corroborating assignments, especially those due to the large shifts induced by the heme. Assignment of NOESY cross peaks was greatly facilitated by a prediction of intensities using a complete relaxation matrix analysis based on the crystal structure. These results suggest that the single-crystal X-ray structure closely resembles that of the solution structure although there is evidence that the solution structure has a more dynamic character.

Cytochrome b_5 is a low-spin electron-transfer hemoprotein that carries out a variety of important physiological functions [for a review, see Mathews and Czerwinski (1976)]. It exists in a membrane-bound and water-soluble form. The membrane-bound form has an additional hydrophobic α-helical domain that anchors the protein to the lipid bilayer. Two similar membrane-bound forms (MW approximately 16K) exist: one is localized to the endoplasmic reticulum while the other is found in the mitochondrial membrane (Strittmatter & Velick, 1956; Lederer et al., 1983). In the endoplasmic reticulum cytochrome b_5 provides reducing equivalents for fatty acid desaturation and cholesterol biosynthesis (Oshino, 1978) and for the oxidation of certain substrates by cytochrome P-450 (Canova-Davis & Waskell, 1984; Pompon & Coon, 1984; Vatsis et al., 1982; Kuwahara & Omura, 1980; Noshiro et al., 1979). The role of cytochrome b_5 in the cytochrome P-450 system appears to be in providing the second of two electrons required for the oxidation of certain substrates (Hildebrandt & Estabrook, 1971). The function of the mitochondrial form is unknown. The soluble form of the protein (MW approximately 10K) occurs naturally in erythrocytes where it functions to reduce methemoglobin (Hegesh et al., 1986). In the studies described here, we utilized a soluble form of cytochrome b_5 obtained by mild trypsin treatment of hepatic microsomes. This trypsin-solubilized form of the protein, although somewhat smaller, is highly homologous to the water-soluble form of the protein found naturally in erythrocytes (Abe et al., 1985).

The trypsin-solubilized form of cytochrome b_5 is an ideal candidate for study by high-resolution NMR[1] spectroscopy because of its marked thermal stability, high solubility, low molecular weight, and ease of purification of large quantities. Recently, a number of studies have been performed resulting in the assignment of the majority of the heme resonances and a number of protein side-chain methyl resonances (Keller et al., 1976; Keller & Wüthrich, 1980; LaMar et al., 1981; McLachlan et al., 1986). One of the earliest high-resolution NMR experiments (Keller & Wüthrich, 1980) clearly demonstrated that the solution structure differed from the single-crystal X-ray structure (Mathews et al., 1972) in the orientation of the heme group. Later it was found that the solution structure consists of a mixture of isomeric forms which differ in orientation of heme binding by a 180° rotation about the α,γ-meso axis (McLachlan et al., 1986). The lower abundance conformer that corresponds to the originally reported crystal structure was found to exist in a ratio of about 1:8 relative to the major abundance form.

Two-dimensional NMR methods have also been applied to the study of the oxidized protein in D_2O (Reid et al., 1987), resulting in the assignment of many of the aromatic resonances. More recently, a study of both oxidized and reduced forms

† Supported by National Institutes of Health Grants GM 35533 (L.W.), GM 19267 (I.D.K.), and RR 1695 (I.D.K.) and by a Veterans Administration Merit Review (L.W.). The UCSF Magnetic Resonance Laboratory was partially funded by grants from the National Science Foundation (DMB 8406826) and the National Institutes of Health (RR-01668).

* Correspondence should be addressed to this author at the Department of Anesthesia (129), Veterans Administration Medical Center, 4150 Clement St., San Francisco, CA 94121.

‡ Department of Anesthesia and Liver Center, University of California, San Francisco, and Anesthesiology Service, Veterans Administration Medical Center.

§ Department of Pharmaceutical Chemistry, University of California, San Francisco.

[1] Abbreviations: NMR, nuclear magnetic resonance; TSP, sodium (trimethylsilyl)propionate; NOE, nuclear Overhauser effect; NOESY, 2D NOE spectroscopy; COSY, 2D correlated spectroscopy; HOHAHA, 2D homonuclear Hartmann-Hahn spectroscopy; t_1, evolution time; t_2, data acquisition time; ω_1, Fourier transformed t_1 data; ω_2, Fourier transformed t_2 data; CORMA, complete relaxation matrix analysis; MCD, main chain directed; ppm, parts per million.

0006-2960/90/0429-1276$02.50/0

of the trypsin-solubilized bovine protein in H_2O reported the assignment of approximately 35% of the chemical shifts of the amide and C^α proton resonances (Veitch et al., 1988). With the exception of the amide resonance of Leu-36, our results confirm these assignments. The results presented here extend these assignments to a set of more than 400 protein proton assignments.

Two-dimensional NMR spectroscopy has been demonstrated to be a useful tool in deducing the solution structures of low molecular weight proteins (Wüthrich, 1986). The determination of a complete set of sequence-specific resonance assignments presented here is the first step toward determining the solution structure of cytochrome b_5. Once the structure of cytochrome b_5 has been determined, a series of additional experiments examining complexes between cytochrome b_5 and other electron-transfer proteins are possible.

Materials and Methods

Isolation and Characterization of Cytochrome b_5. Trypsin-solubilized cytochrome b_5 was isolated from liver microsomes obtained from calf, rabbit, and pig according to the procedure described by Reid and Mauk (1982). All purified cytochrome b_5 preparations exhibited A_{413}/A_{280} ratios greater than or equal to 5.85 and showed a single band on SDS–polyacrylamide gels. The rabbit cytochrome b_5 preparation as initially isolated was found to be a mixture of two forms. Only the lower molecular weight form was used in the NMR studies. The amino terminus of the rabbit protein was determined to be an aspartate by an Edman degradation while the amino terminus of the bovine protein was determined to be an alanine (Altman et al., 1989). The carboxy termini of the rabbit and bovine proteins were determined by mass spectrometry to be Arg-84 (B. Gibson, A. Fallick, J. J. Lipka, and L. Waskell, unpublished results).

NMR Sample Preparation. The purified proteins were desalted over a coarse G-25 column and lyophilized from a 100 mM ammonium bicarbonate solution. The fact that cytochrome b_5 contains a noncovalently bound heme leads to a number of experimental difficulties. The reduced protein has a limited range of pH stability due to reversible loss of the heme. For example, it was found that approximately 10% of the heme dissociated from the reduced protein at pH 6.5. As a result, all NMR samples were prepared by dissolving lyophilized cytochrome b_5 in 100 mM pH 7 phosphate buffers prepared in either 90% H_2O (10% D_2O) or 99.96% D_2O. Cytochrome b_5 samples prepared in 99.96% D_2O buffers were lyophilized twice from 99.96% D_2O prior to dissolution in the final phosphate buffer. Small adjustments in the pD to a final value of 7.2 were made by additions of small aliquots of 0.25 M NaOD or DCl. Measurements of pH were not corrected for isotope effects. (Trimethylsilyl)propionic acid (TSP) was added to a final concentration of 1 mM as an internal chemical shift reference. Cytochrome b_5 solutions were reduced by addition of a small quantity of solid sodium dithionite. The protein solutions were purged with argon prior to the addition of the sodium dithionite, and then the NMR tubes were sealed under vacuum with a gas–oxygen torch. Cytochrome b_5 concentrations between 5 and 10 mM were used in all NMR experiments. Concentrations of the ferric protein were determined with an absorption coefficient of 117 mM^{-1} at 413 nm (Strittmatter & Velick, 1956).

Two-Dimensional NMR Spectra. NMR spectra were recorded on a 500-MHz General Electric GN-500 NMR spectrometer interfaced to a Nicolet 1280 computer. All spectra were recorded in the phase-sensitive mode with quadrature detection in both dimensions. The majority of the two-dimensional spectra were recorded at 40 °C although some bovine NOESY spectra were recorded at 20 °C in order to take advantage of the temperature-dependent chemical shift of amide proton resonances. NOESY spectra were acquired with the method of States et al. (1982). Mixing times of 100 and 200 ms were used. Relaxation delay times of 3.5 s were used in all cases. Double-quantum filtered COSY (Piantini et al., 1982; Shaka & Freeman, 1983) spectra were acquired with time proportional phase incrementation of the first pulse (Redfield & Kunz, 1975). HOHAHA spectra using the MLEV-17 spin lock sequence (Bax & Davis, 1985) were acquired by use of a transmitter equipped with a 6- or 10-W high-power amplifier. Mixing times of 50, 75, and 100 ms were used. For some HOHAHA spectra recorded in H_2O the transmitter frequency was offset from the water resonance to the low-field side. Offsetting the transmitter in this manner was found to yield improved sensitivity for some of the amide relay ladders that were associated with amide protons with unusually low field resonances. Suppression of the water resonance in H_2O was generally accomplished by continuous irradiation during the relaxation delay. However, for some NOESY spectra, the water signal was suppressed with the 1331 method (Hore, 1983). Phase-sensitive double-quantum filtered COSY spectra were collected with 1024 t_1 increments and were zero filled to 1024 data points with 4096 points in ω_2. All other spectra were acquired with 512 t_1 and zero filled in t_1 to give a real matrix of 1024 points by 2048 points in ω_2. All spectra were recorded with a spectral width of 7246 Hz.

Data Analysis. Two-dimensional NMR spectra were transferred to Sun Microsystems 3/160 workstations running a UNIX operating system. Two-dimensional NMR spectra were processed on software originally developed in the laboratory of Dr. Kaptein at the University of Groningen, Groningen, The Netherlands. Many modifications and improvements have been made by Dr. R. M. Scheek, Dr. S. Manogaran, and Mr. M. Day in our laboratory. In all cases a 45° phase-shifted sine bell was applied in t_2 prior to Fourier transformation. For all double-quantum filtered COSY experiments a 70° phase-shifted sine-squared bell was used in t_1. For NOESY and HOHAHA spectra Gaussian filters with line-broadening parameters of 5–7 Hz were used. Automatic base-line correction of H_2O spectra was accomplished by an adaptation of an algorithm originally described by Pearson (1977). The intensities of NOESY cross peaks were calculated with a complete relaxation matrix analysis (CORMA) program developed by Keepers and James (1984). The single-crystal X-ray structure (Mathews et al., 1972) was used in the calculation. Idealized proton coordinates were generated from the heavy atom positions with a computer program from the James laboratory. A correlation time of 6 ns was assumed. This value is slightly longer than that typical of spherical globular proteins (Cantor & Schimmel, 1980) because of the more cylindrical structure of cytochrome b_5. Ring-current shifts were determined with a program originally written by Dr. Keith Cross at the Research Institute of Scripps, La Jolla, CA. It is based on a classical superconducting loop approximation (Johnson & Bovey, 1958).

Results

Outline of Assignment Approach. Sequence-specific proton resonance assignments were determined largely by methods developed by Wüthrich and co-workers (Billeter et al., 1982; Wüthrich et al., 1984). Our assignment approach differed somewhat from the exact procedure described by Wüthrich and co-workers. For example, instead of defining side-chain amino acid spin systems via through-bond correlations in D_2O,

we began by assigning main-chain resonances in H_2O. Much of the laborious task of assigning a set of main-chain spin systems was accomplished in an automated manner. A program developed in our laboratory (Eads & Kuntz, 1989), which used COSY and HOHAHA peak coordinates as input, rapidly facilitated the assignment of the majority of the main-chain spin systems. Side-chain resonances of these arbitrarily labeled amino acid spin systems were then systematically identified by tracing characteristic patterns of through-bond scalar coupling networks. Long-range coherence transfers observed in HOHAHA spectra made side-chain assignments much easier than dependence on COSY spectra alone.

Because the primary sequence of cytochrome b_5 is known, it was possible to obtain sequence-specific resonance assignments as described above. For the most part, expected NOESY connectivities between sequential residues were observed that were characteristic of regions of well-defined secondary structure (Wüthrich et al., 1984). However, in regions of distorted secondary structure we found that estimates of relative NOESY peak intensities calculated from a complete relaxation rate matrix analysis with coordinates from the crystal structure were of predictive value for sequential assignment. Resonance assignments were also predicted or corroborated by examining the effect of aromatic ring-current fields on the resonance positions of protons near aromatic residues, again on the basis of the single-crystal X-ray structure.

Although two-dimensional NMR spectroscopy overcomes what would have been an impossible assignment problem for one-dimensional techniques, still the major problem associated with the assignment of a protein the size of cytochrome b_5 is the deconvolution of coincident resonances or overlapping peaks. For cytochrome b_5 this was accomplished primarily by examining differences between proteins isolated from different species and by varying the temperature at which the NMR spectra were acquired. Examination of coincident resonances for the arbitrarily labeled fingerprint peaks (i.e., C^α proton to amide proton cross peaks in the H_2O COSY spectrum) of bovine cytochrome b_5 at 40 °C yielded multiple assignment possibilities for about 80% of the spin systems within a tolerance of ±0.02 ppm. Temperature-dependent variation of amide resonances resulted in shifts that reduced the level of ambiguity in amide resonances to 27%. Differences between porcine and bovine cytochrome b_5 spectra further reduced the level of ambiguity to 15%. It is important to note that the relatively small number of amino acid differences (see Table I) between the pig and calf proteins produced significant differences in amide proton resonances significantly removed from the sites of substitution. The C^α proton resonances overlapped more than the amide resonances. Ambiguities in the assignment of C^α proton resonances were reduced to 59% after examination of temperature-dependent shifts. Differences between bovine and porcine spectra reduced this level of ambiguity to 27%. Further deconvolution of aligned resonances was achieved by comparisons with the rabbit cytochrome b_5 spectra and by observation of unambigous heme to protein proton NOESY connectivities. Once these chemical shift ambiguities had been resolved, a virtually complete set of sequence-specific assignments was obtained for the bovine and porcine cytochrome b_5 proteins by two-dimensional methods described in detail below. Sequence-specific assignments are summarized in Table I (see also Figure 1). The broad range of C^α and amide proton resonances evident in Figure 1 is largely a consequence of ring-current shifts caused by the heme. As described below, ring-current calculations based on the X-ray crystal structure were useful in predicting or confirming many of the protein proton resonances.

Main-Chain Spin System Identification. An automated approach developed in our laboratory by Dr. C. Eads (Eads & Kuntz, 1989) was taken in the assignment of the main-chain (i.e., C^α, C^β, and amide proton) resonances of amino acid spin systems. These were initially identified with arbitrary labels which were assigned to fingerprint peaks (e.g., C^α proton to amide proton cross peaks found in the H_2O COSY spectra). Generally, a single fingerprint peak is observed for each amino acid, although glycines often have nonequivalent C^α proton resonances. Prolines are another exception. They lack amide protons and do not exhibit fingerprint peaks. However, for cytochrome b_5 there are a number of cases where expected fingerprint peaks were not observed (e.g., see Figure 1, His-80, Thr-55, His-39, Leu-36, and Thr-33) presumably because of a small $^3J_{N\alpha}$ coupling constant (see below). The appropriate resonances were seen in the NOESY spectra.

As much as possible, assignment of individual amino acid spin systems was based on scalar coupling networks alone. The automated procedure involved systematic searches through COSY and HOHAHA peak coordinate files as follows. First, the centroids of peaks in the C^α proton to amide proton and C^α proton to C^β proton regions of the COSY spectrum were determined by integration of cross peaks. The limits of integration for each cross peak were determined manually by an interactive graphics program. Similarly, peak coordinate files were generated for the amide proton region of the HOHAHA spectra. Once these coordinate files had been assembled, systematic searches within a set tolerance (e.g., usually ±0.02 ppm) for relay peaks of a given spin system were performed for each fingerprint peak. Once a relay peak had been identified in the H_2O HOHAHA, a search through the COSY C^α proton to C^β proton cross-peak coordinate file was performed. If a C^α proton to C^β proton cross peak was found, a C^β proton resonance was clearly identified. In this manner 86 spin systems were identified of which 61 had been assigned one or more C^β protons. Note that for an 82-residue protein with two prolines and six glycines one would expect 80–86 fingerprint peaks.

Side-Chain Spin System Identification. A systematic search for side chains was undertaken in the following order: glycines, alanines, threonines, serines, leucines, isoleucines, aromatics, long side chains (e.g., arginines, lysines, and prolines), and finally acidic residues (Basus, 1989).

Glycines can often be identified on the basis of the observation of two fingerprint peaks aligned along the same amide resonance and which correspond to an intense peak with characteristic multiplet structure due to the large C^α proton to $C^{\alpha\prime}$ proton coupling constant. Three of the six glycines were readily identified in this manner in the bovine spectra. Note that only one of each of these fingerprint peaks is visible in the double-quantum filtered COSY spectrum of the porcine protein shown in Figure 1. Of the three remaining glycines, two exhibited the expected additional fingerprint peak in the HOHAHA spectra. The observation of these weaker or missing COSY peaks in the HOHAHA spectra has been noted before (Basus et al., 1988) and is due to the efficient transfer of magnetization between C^α protons due to the large C^α–$C^{\alpha\prime}$ proton coupling. It is interesting to note the distribution of glycines within the primary sequence of the protein. There are two pairs of sequentially connected glycines and two isolated glycines. One of the two pairs (Gly-41 and Gly-42) is located close to the heme as is indicated by the substantial ring

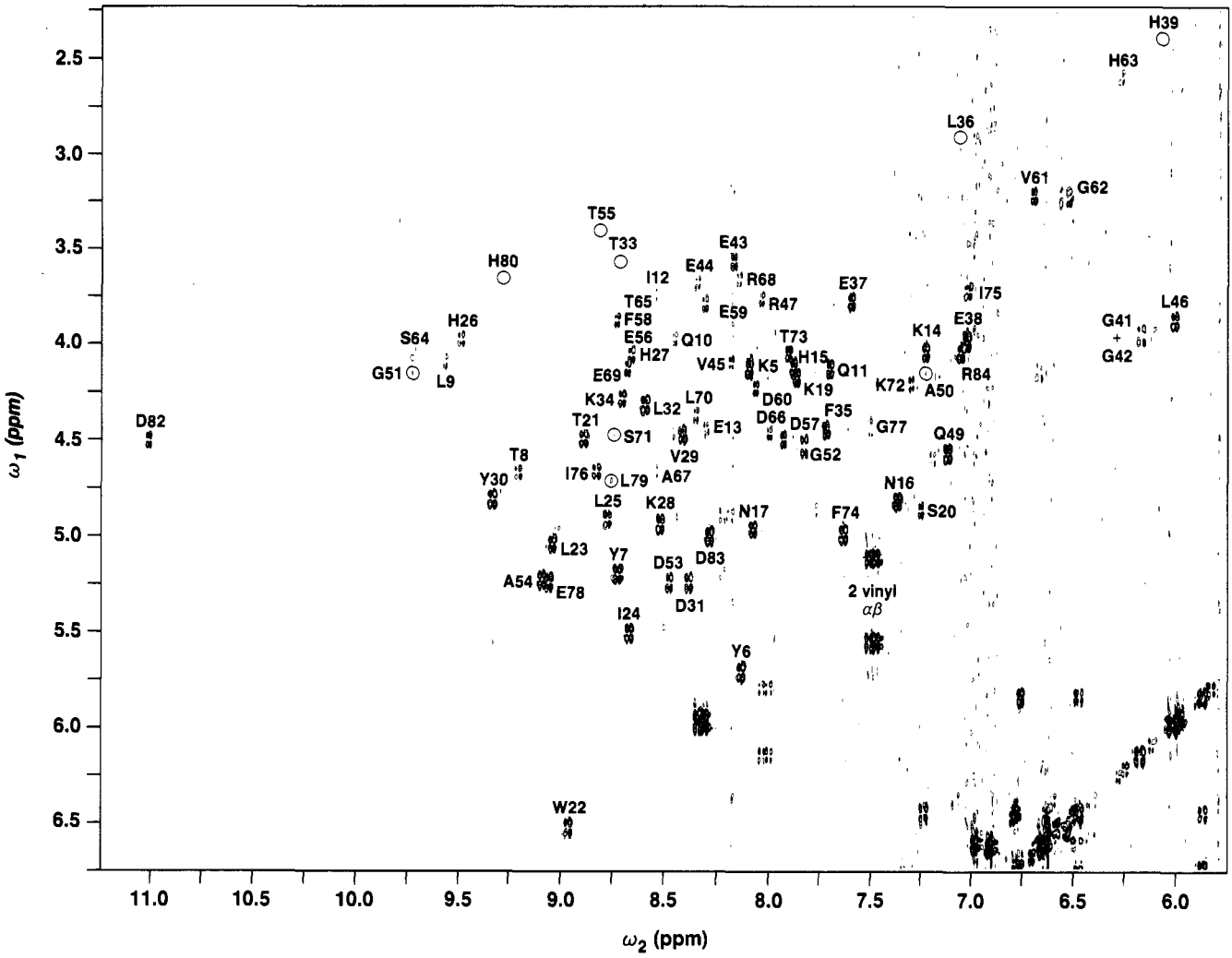

FIGURE 1: Contour plot of the fingerprint region (ω_1 = 2.25–6.75 ppm, ω_2 = 5.75–11.25 ppm) of a double-quantum filtered COSY spectrum of porcine cytochrome b_5 (10 mM) recorded in H_2O at 40 °C. The $C^\alpha H$–NH cross peaks are labeled with sequence-specific assignments. The single-letter amino acid abbreviations used are listed in Table I. Circles are used to clarify positions of a few weak peaks or to indicate positions of peaks determined from other spectra. Both positive and negative contour levels are shown.

shift of the amide resonances. Similarly, only one of the two isolated glycines (Gly-62) is located near the heme while the other isolated glycine did not exhibit significant ring-shift effects. The assignment of Gly-41 was complicated in the bovine protein for two reasons: First, the amide resonances of Gly-41 and Gly-42 are virtually identical in both the bovine and porcine spectra, and the bovine spectra are further obscured by the overlap of the His-63 amide resonances. Second, one of the C^α proton resonances of Gly-41 exhibits an anomalously large ring-current shift (e.g., nearly 4 ppm) due to the heme. However, this assignment is unambiguous given the COSY peak with characteristic multiplet structure in the region near 0.3 ppm (see Figure 2).

Three of the four alanines were readily identified on the basis of the alignment of fingerprint C^α proton resonances with intense C^α proton to C^β methyl proton cross peaks. The remaining alanine, Ala-3 (the amino-terminal residue), was associated with an appropriate cross peak which was present in the bovine and porcine spectra but absent from the rabbit spectra in which the alanine is replaced by an aspartic acid. The amino-terminal amino proton resonances were not observed, presumably due to rapid exchange with the solvent.

The HOHAHA experiment was an extremely useful tool in rapidly identifying all long side-chain spin systems through the observation of characteristic ladders of cross peaks. For example, three of the six threonines (Thr-21, -65, and -73) were readily identified by the presence of two peaks in the fingerprint region of the HOHAHA spectrum and the alignment of an intense C^β proton to C^γ methyl proton cross peak with the amide proton to C^β proton relay peak in the HOHAHA spectrum. Thr-55 and Thr-33 were unusual in that they did not exhibit fingerprint peaks in either the H_2O COSY or HOHAHA spectrum, presumably due to a very small coupling between C^α and amide protons. However, intense peaks in the HOHAHA spectrum corresponding to C^β proton to C^γ methyl proton cross peaks and C^α proton to C^γ proton relay cross peaks (see Figure 3) could be associated with C^α proton to amide proton and C^β proton to amide proton cross peaks in the fingerprint region of the H_2O NOESY spectrum. The presence of an intense $C^\gamma H$ to amide proton cross peak in the NOESY spectrum provided additional support for these assignments. Assignment of the C^α proton and C^β proton resonances of Thr-55 are in good agreement with previous assignments based on one-dimensional NOE experiments in D_2O (Keller & Wüthrich, 1980). The amide proton resonance of Thr-33 was coincident with the Lys-34 amide proton resonance at 40 but not at 20 °C. Unambiguous midrange NOESY cross peaks observed between residues 33 and 36 and residues 34 and 37 in this helical segment of the protein (see sequential assignments below) confirmed these spin system assignments. The Thr-8 COSY fingerprint peak was also not observed in the bovine spectra at 40 °C because the C^α proton resonance

Table I: Summary of Sequence-Specific Proton Resonance Assignments for Cytochrome b_5[a]

residue[b]	NH	$C^{\alpha}H$	$C^{\beta}H$	$C^{\beta'}H$	other assignments
A3[c][D3]	NA	4.01 (4.10)	1.30 (1.32)		
V4	NA	3.88 (3.90)	1.62 (1.48)		0.66 ($C^{\gamma}H$) 0.38 ($C^{\gamma'}H$)
K5	8.04 (8.07)	4.10 (4.13)	1.63 (1.66)		1.41 ($C^{\gamma}H$) 1.76 ($C^{\gamma}H$) 2.91 ($C^{\epsilon}H$)
Y6	8.09 (8.11)	5.72 (5.72)	2.84 (2.88)	2.67 (2.69)	6.86 ($C^{\delta}H$) 6.59 ($C^{\epsilon}H$)
Y7	8.74 (8.72)	5.18 (5.18)	3.23 (3.23)	2.54 (2.55)	6.96 ($C^{\delta}H$) 6.59 ($C^{\epsilon}H$)
T8	9.19[d] (9.21)	4.66[d] (4.66)	4.90 (4.90)		1.22 ($C^{\gamma}H$)
L9	9.57 (9.56)	4.10 (4.10)	1.76 (1.79)	1.63 (1.66)	1.77 ($C^{\gamma}H$) 1.04 ($C^{\gamma}H$) 1.08 ($C^{\gamma'}H$)
E'10 (Q10)	8.43 (8.44)	3.96 (3.98)	1.99 (1.99)	2.06 (2.06)	2.32 ($C^{\gamma}H$)
Q11	7.67 (7.67)	4.12 (4.13)	2.33 (2.34)		2.72, 2.47 ($C^{\beta'}H$, $C^{\gamma}H$)
112	8.53 (8.44)	3.73 (3.74)	2.00 (2.00)		1.59 ($C^{\gamma}H$) 0.94 ($C^{\gamma}H_3$) 0.87 ($C^{\delta}H$)
E13 ([K13]	8.30[e] (8.29)	4.44[e] (4.46)	2.22 (2.25)		2.66 ($C^{\gamma}H$)
K14	7.21 (7.20)	4.04 (4.05)	1.48 (1.46)	1.61 (1.61)[e]	1.36 ($C^{\gamma}H$) 1.73 ($C^{\delta}H$) 2.92 ($C^{\epsilon}H$)
H15	7.87 (7.84)	4.04 (4.05)	2.53 (2.52)	2.07 (2.09)[e]	6.96 ($C^{\delta}H$) 7.93 ($D^{\epsilon}H$)
N16	7.34 (7.34)	4.83 (4.84)	2.37 (2.39)	3.04 (3.02)	
N17 [H17]	8.03[e] (8.05)	4.96[e] (4.98)	3.09 (3.14)	2.72 (2.76)	
S18	7.36	4.63	4.19		
K19	7.83 (7.84)	4.17 (4.17)	1.74 (1.75)	1.79 (1.82)	1.33 ($C^{\gamma}H$) 1.41 ($C^{\gamma'}H$) 1.60 ($C^{\delta}H$) 2.93 ($C^{\epsilon}H$)
S20	7.20 (7.22)	4.87 (4.88)	3.56 (3.59)	3.85 (3.85)	
T21	8.88 (8.88)	4.48 (4.50)	3.60 (3.63)		0.93 ($C^{\gamma}H$)
W22	8.95 (8.96)	6.52 (6.53)	3.23 (3.22)	3.02 (3.04)	6.72 ($C^{\epsilon_3}H$) 5.83 ($C^{\zeta_3}H$) 6.41 ($C^{\eta_2}H$) 6.72 ($C^{\zeta_2}H$) 6.96 ($C^{\delta_1}H$) 8.77 ($N^{\epsilon_1}H$)
L23	8.99 (9.04)	5.05 (5.05)	2.24 (2.26)		1.85 ($C^{\gamma}H$) 1.06 ($C^{\delta}H$) 1.02 ($C^{\delta'}H$)
124	8.64 (8.66)	5.52 (5.52)	1.72 (1.72)		0.95 ($C^{\gamma}H$) 0.90 ($C^{\gamma'}H$) 0.92 ($C^{\gamma}H_3$)
L25	8.86 (8.77)	4.91 (4.92)	1.91 (1.89)		1.11 ($C^{\gamma}H$) 0.64 ($C^{\delta}H$) −0.45 ($C^{\delta'}H$)
H26	9.46 (9.48)	3.86 (3.99)	3.26 (3.19)	3.21 (3.20)	7.00 ($C^{\delta}H$) 8.33 ($C^{\epsilon}H$)
Y27 (H27)	8.34 (8.65)	3.89 (4.06)	2.66 (3.19)	3.56	7.11 ($C^{\delta}H$) 7.02 ($C^{\epsilon}H$)
K28	8.44 (8.51)	4.89 (4.95)	2.37 (2.37)		1.54 ($C^{\gamma}H$) 1.76 ($C^{\delta}H$) 3.07 ($C^{\epsilon}H$)
V29	8.46 (8.40)	4.47 (4.49)	1.21 (1.25)		0.76 ($C^{\gamma}H$) 0.30 ($C^{\gamma'}H$)
Y30	9.33 (9.37)	4.80 (4.83)	2.92 (2.94)	2.65 (2.64)	7.28 ($C^{\delta}H$) 6.89 ($C^{\epsilon}H$)
D31	8.37 (8.37)	5.23 (5.25)	3.05 (3.02)	1.96 (1.94)	
L32	8.55 (8.58)	4.30 (4.33)	1.61 (1.60)		1.60 ($C^{\gamma}H$) 0.93 ($C^{\delta}H$) 0.60 ($C^{\delta'}H$)
T33	8.66[d] (8.70)[d]	3.53 (3.55)	4.24 (4.27)		1.25 ($C^{\gamma}H$)
K34	8.65 (8.69)	4.28 (4.29)	1.81 (1.84)		1.73, 2.21 ($C^{\beta'}H$, $C^{\gamma}H$) 1.60 ($C^{\delta}H$) 3.05 ($C^{\epsilon}H$)
F35	7.67 (7.70)	4.43 (4.46)	2.45 (2.47)	1.96 (1.98)	6.60 ($C^{\delta}H$) 6.44 ($C^{\epsilon}H$) 7.19 ($C^{\zeta}H$)
L36	7.03[d] (7.04)[d]	2.95 (2.96)	1.55 (1.60)		1.74 ($C^{\gamma}H$) 0.75 ($C^{\delta}H$) 0.49 ($C^{\delta'}H$)
E37	7.54 (7.57)	3.78 (3.78)	1.72 (1.76)	1.88	2.07 ($C^{\gamma}H$)
E38	7.00 (7.00)	3.99 (3.99)	2.07 (1.99)	1.58 (1.62)	1.83 ($C^{\gamma}H$)
H39	6.01 (6.04)	2.46 (2.46)	0.81 (0.81)	0.48 (0.48)[c]	
P40	NA	3.56 (3.56)	1.62 (1.62)		1.66 ($C^{\gamma}H$) 3.71 ($C^{\delta}H$) 1.25 ($C^{\delta'}H$)
G41	6.13 (6.15)	3.34 (3.35)			0.32 (0.34) ($C^{\alpha'}H$)
G42	6.13 (6.14)	3.34 (3.36)			3.93 (3.96) ($C^{\alpha'}H$)
E43	8.09 (8.15)	3.56 (3.56)	1.63 (1.65)	1.72 (1.75)	1.88 ($C^{\gamma}H$)
E44	8.25 (8.33)	3.67 (3.69)	1.93 (1.95)		2.21 ($C^{\gamma}H$)
V45	8.15 (8.16)	4.07 (4.09)	2.55 (2.57)		1.00 ($C^{\gamma}H$) 0.77 ($C^{\gamma'}H$)
L46	5.96 (5.98)	3.86 (3.88)	1.44 (1.46)	0.56	0.19 ($C^{\gamma}H$) −0.70 ($C^{\delta}H$) −0.76 ($C^{\delta'}H$)
R47	8.00 (8.01)	3.75 (3.76)	1.72 (1.75)		1.49 ($C^{\gamma}H$) 3.03 ($C^{\delta}H$)
E48	8.04 (8.07)	4.10 (4.13)	2.14 (2.16)		2.49 ($C^{\gamma}H$)
Q49	7.09 (7.09)	4.58 (4.60)	1.94 (1.96)		2.71 ($C^{\gamma}H$)
A50	7.22 (7.25)	4.18 (4.20)	1.26 (1.28)		
G51	9.71 (9.73)	4.14 (4.16)			3.80 (3.80) ($C^{\alpha'}H$)
G52	7.78 (7.80)	4.53 (4.54)			3.87 (3.89) ($C^{\alpha'}H$)
D53	8.44 (8.46)	5.21 (5.25)	3.05 (3.15)		
A54	9.03 (9.09)	5.21 (5.24)	1.78 (1.81)		
T55	8.60[d] (8.74)	3.32[d] (3.37)	4.01 (4.05)		0.40 ($C^{\gamma}H$)
E56	8.66 (8.75)	3.85 (3.88)	1.97 (1.98)		2.21 ($C^{\gamma}H$) 2.28 ($C^{\gamma'}H$)
D57 (N57)	7.92 (7.90)	4.48 (4.50)	2.83 (2.85)	3.22 (3.25)	
F58	8.66 (8.72)	3.85 (3.88)	2.91 (2.95)	1.98 (1.99)	7.30 ($C^{\epsilon}H$) 7.01 ($C^{\delta}H$) 7.36 ($C^{\zeta}H$)
E59	8.22 (8.29)	3.79 (3.80)	1.85 (1.90)		2.00 ($C^{\gamma}H$)
D60	8.07 (8.04)	4.21 (4.23)	2.55 (2.58)	2.75 (2.77)	
V61	6.65 (6.67)	3.22 (3.22)	0.23 (0.25)		0.79 ($C^{\gamma}H$) −1.23 ($C^{\gamma'}H$)
G62	6.50 (6.50)	3.38 (3.38)			3.17 (3.17) ($C^{\alpha'}H$)
H63	6.15 (6.25)	2.57 (2.60)	1.10 (1.12)	0.38 (0.39)	0.35 ($C^{\delta}H$) 0.78 ($C^{\epsilon}H$)
S64	9.72 (9.72)	4.06 (4.08)	4.28 (4.25)		
T65	8.66 (8.72)	3.79 (3.88)	4.18 (4.22)		1.26 ($C^{\gamma}H$)
D66	7.96 (7.97)	4.46 (4.47)	2.87 (2.87)		
A67	8.53 (8.53)	4.66 (4.67)	1.21 (1.23)		
R68	8.09 (8.12)	3.64 (3.66)	1.75 (1.75)		1.69, 1.36 ($C^{\beta'}H$, $C^{\gamma}H$)
E69	8.65 (8.66)	4.14 (4.13)	2.20 (2.24)	1.74 (1.76)	2.38 ($C^{\gamma}H$)
L70	8.33 (8.33)	4.34 (4.37)	2.64 (2.68)	2.10 (2.10)	1.87 ($C^{\gamma}H$) 0.81 ($C^{\delta}H$) 1.19 ($C^{\delta'}H$)
S71	8.69 (8.75)	4.50 (4.52)	4.12 (4.14)	3.35 (3.36)	
K72	7.27 (7.28)	4.19 (4.23)	1.96 (1.99)		1.74, 1.84 ($C^{\beta'}H$, $C^{\gamma}H$) 1.60 ($C^{\delta}H$) 3.18 ($C^{\epsilon}H$)
T73	7.86 (7.88)	4.03 (4.06)	3.78 (3.74)		1.09 ($C^{\gamma}H$)
F74	7.58 (7.61)	5.00 (5.01)	3.00 (3.02)		7.30 ($C^{\delta}H$) 6.88 ($C^{\epsilon}H$) 7.03 (ζ)
I75	6.99 (6.99)	3.72 (3.72)	1.59 (1.59)		0.95 ($C^{\delta}H$) 0.87 ($C^{\gamma}H_3$) −0.02 ($C^{\gamma}H$)
I76	8.84 (8.82)	4.66 (4.67)	1.88 (1.77)		0.12 ($C^{\gamma}H$) 0.32 ($C^{\gamma'}H_3$) 0.82 ($C^{\gamma}H_3$) −1.01 ($C^{\delta}H$)
G77	7.46 (7.48)	4.47 (4.47)			4.13 (4.16) ($C^{\alpha'}H$)
E78	9.04 (9.06)	5.30 (5.25)	1.74	1.88 (1.87)	2.22 ($C^{\gamma}H$)
L79	8.97 (9.07)	4.73 (4.70)	1.85		2.22 ($C^{\gamma}H$) 1.02 ($C^{\delta}H$) 0.97 ($C^{\delta'}H$)

Table I (Continued)

residue[b]	NH	$C^{\alpha}H$	$C^{\beta}H$	$C^{\beta'}H$	other assignments
H80	9.09[c](9.08)	3.79 (3.82)	2.98 (2.98)	2.60 (2.62)	6.97 ($C^{\delta}H$) 7.58 ($C^{\epsilon}H$)
P81	NA	3.67 (3.74)	2.12 (2.17)		1.50 ($C^{\gamma}H$) 2.18 ($C^{\delta}H$) 2.72 ($C^{\delta'}H$)
D82	11.03 (11.02)	4.48 (4.50)	2.66 (2.67)	2.73 (2.74)	
D83	8.23 (8.26)	5.00 (5.01)	2.67 (2.68)	3.14 (3.12)	
R84	7.03 (7.03)	4.11 (4.05)	1.65 (1.66)		1.63 ($C^{\gamma}H$) 2.81 ($C^{\delta}H$)

[a] Numbers in parentheses refer to porcine cytochrome b_5 assignments. [b] Primary amino acid sequences from Mathews et al. (1979). Amino acids found in the porcine protein are indicated in parentheses. Amino acids found in the rabbit protein are indicated in square brackets. Abbreviations: A, Ala; D, Asp; E, Glu; E', Glx; F, Phe; G, Gly; H, His; I, Ile; K, Lys; L, Leu; N, Asn; P, Pro; Q, Gln; R, Arg; S, Ser; T, Thr; V, Val° W, Trp; Y, Tyr. [c] This assignment is based on differences between bovine, rabbit, and porcine spectra. [d] Assignment based on NOESY data alone. [e] These assignments are supported by differences between rabbit and bovine spectra.

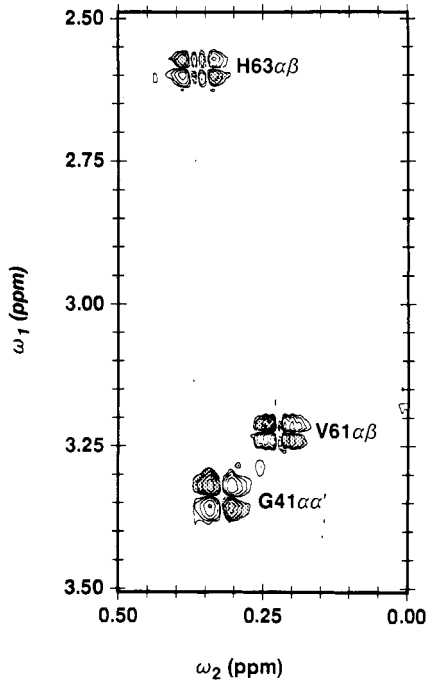

FIGURE 2: Contour plot of a region of a double-quantum filtered COSY of bovine cytochrome b_5 recorded at 40 °C in D_2O. This region contains several C^{α}–$C^{\alpha'}$ or C^{α}–C^{β} proton cross peaks that were markedly shifted by the heme.

was too close to the water resonance, but it was clearly resolvable in the porcine spectra (see Figure 1).

Following the assignment of the glycines and threonines, two of the four serines could be assigned on the basis of the presence of two peaks aligned along the same amide resonance position in the H_2O HOHAHA spectrum. Ser-64 did not exhibit an amide proton to C^{β} proton cross peak in the HOHAHA spectra, but NOESY amide proton to C^{β} proton cross peaks and COSY C^{α} proton to C^{β} proton cross peaks were found consistent with the assignment of a serine spin system. The Ser-18 C^{α} proton resonance lies right on the water resonance at 40 °C. Assignment of this spin system is tentative and based largely on connectivities between both C^{β} protons of Asn-17 and an amide resonance observed in the H_2O NOESY spectra of the bovine protein.

Three of the four valines (Val-29, -45, and -61) were identified on the basis of amide proton relay peaks out to the C^{γ} protons in the HOHAHA spectra (see Figure 4). The Val-61 C^{γ} proton and C^{β} proton resonance assignments are consistent with previously published assignments based on ring-current shift calculations and one-dimensional NOE studies (Keller & Wüthrich, 1980). The Val-4 amide resonance was not observed, presumably due to rapid exchange. However, peaks in the HOHAHA spectrum are clearly indicative of an additional valine spin system (e.g., two intense $C^{\alpha}H$ to $C^{\gamma}H$ peaks aligned with a previously unassigned $C^{\alpha}H$ to $C^{\beta}H$ cross peak—see Figure 3). NOESY cross peaks due to coupling between these C^{α}, C^{β}, and C^{γ} protons and the amide proton of Lys-5 confirm the assignment of this spin system to Val-4.

Of the 13 aromatic side chains, all but Phe-58 and the axial histidines could be assigned unambiguously on the basis of NOESY cross peaks observed in D_2O between aromatic ring protons and C^{β} and C^{α} protons. The Trp-22 aromatic spin system is unusual in that the C^{ϵ_3} and C^{ζ_2} proton resonances are accidentally coincident. This is evident from the apparent lack of a relay peak from the C^{ζ_3} to the C^{ζ_2} proton resonance position in the HOHAHA spectra. Thus this relay peak must underlie the C^{ϵ_3} to C^{ζ_3} proton cross peak.

The assignment of Phe-58 was complicated for two reasons: First, the fingerprint peaks of Glu-56 and Phe-58 are coincident in both bovine and porcine spectra. This overlap was confirmed on the basis of the observation of midrange connectivities between Glu-56 and Glu-59 within this helical segment and by the observation of expected heme proton NOESY cross peaks with Phe-58. Second, one of the aromatic resonances of Phe-58 overlapped with an aromatic resonance of Tyr-27.

The main-chain resonances of the axial histidines were initially assigned on the basis of NOESY connectivities to sequential neighbors and were supported by ring-shift calculations. His-63 exhibited a COSY fingerprint peak but His-39 did not. However, a weak fingerprint peak for His-39 is evident in the H_2O HOHAHA spectrum. Once the main-chain resonances of His-63 had been assigned on the basis of sequence-specific connectivities, NOESY cross peaks between the severely ring-shifted aromatic ring protons and the main-chain resonances were identified.

With few exceptions (e.g., most notably Lys-19) the long side chain basic residues did not exhibit amide relay ladders in the HOHAHA spectra beyond the C^{β} protons. These spin systems were mapped out by following single magnetization relay steps in the HOHAHA spectra along the side chain (i.e., amide proton to C^{β} proton relays were used to identify the main-chain proton resonances and then C^{α} to C^{γ} proton relays were used to extend these assignments and so on). In general, side-chain amine, amide, or guanidino nitrogen proton resonances were not observed due to fast exchange at the high pH we used. Thus, glutamines and asparagines were indistinguishable from glutamates and aspartates, respectively. The two prolines apparently both have trans peptide bonds as is evident from the intense $C^{\alpha}H_i$ to $C^{\delta}H_{i+1}$ NOESY cross peaks and the absence of $C^{\delta}H_i$ to $C^{\alpha}H_{i+1}$ and NH_{i-1} to $C^{\alpha}H_i$ peaks (Wüthrich et al., 1984). Once the C^{δ} proton resonances had been assigned, it was possible to trace these spin systems via relays in the D_2O HOHAHA.

The preponderance of acidic residues (e.g., 11 glutamates and 7 aspartates) in cytochrome b_5 made unambiguous assignment of this class of side-chain spin systems virtually

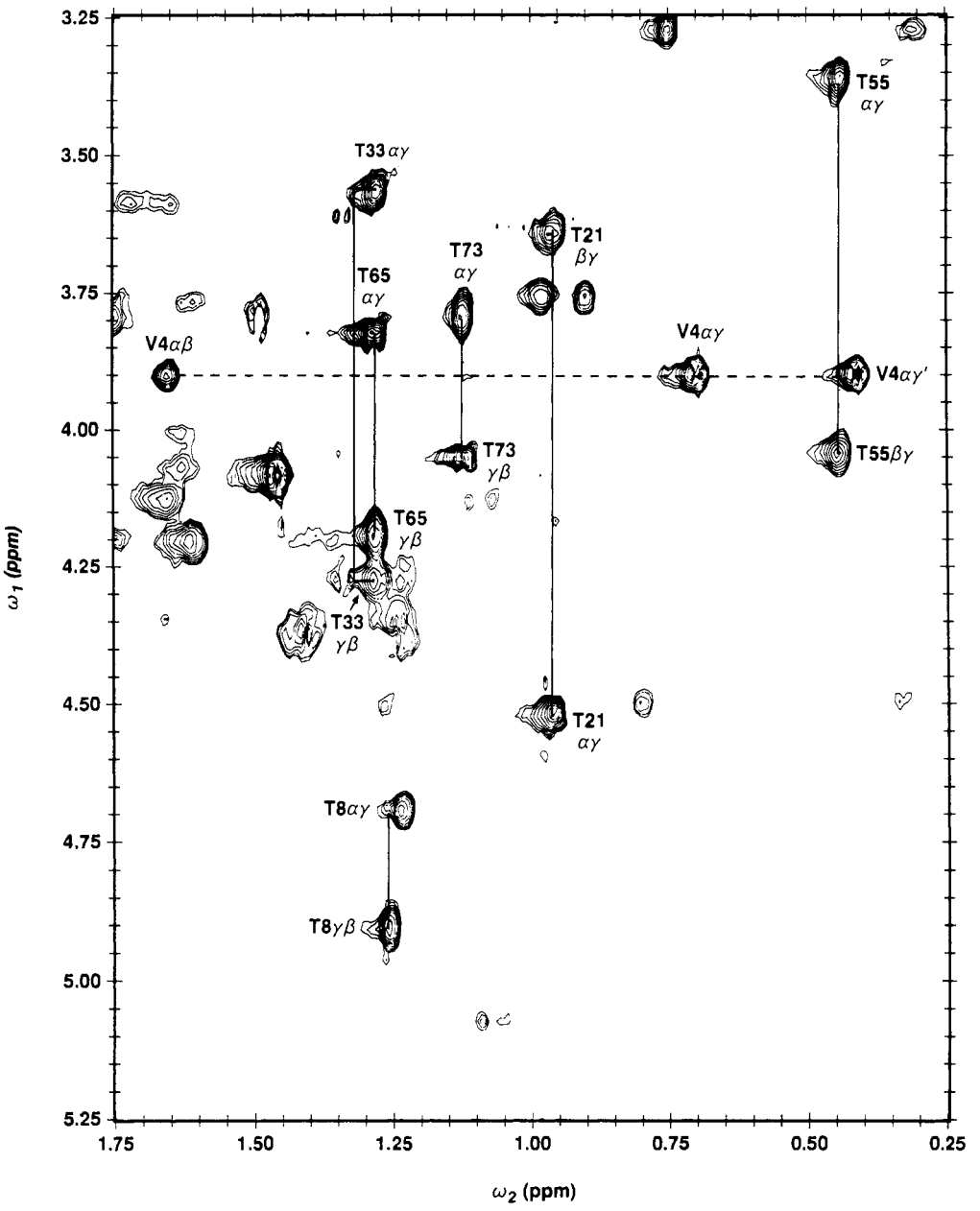

FIGURE 3: Contour plot of a region of the HOHAHA spectrum of bovine cytochrome b_5 recorded at 40 °C in D_2O. The region shown (ω_1 = 0.25–1.75 ppm and ω_2 = 3.25–5.25 ppm) contains direct $C^{\beta}H$–C^{γ} methyl proton cross peaks due to the six threonines and relayed $C^{\alpha}H$–C^{γ} proton cross peaks of these spin systems. Also indicated is the direct $C^{\alpha}H$–$C^{\beta}H$ cross peak of Val-4 and the $C^{\alpha}H$–$C^{\gamma}H$ and $C^{\alpha}H$–$C^{\gamma'}$ proton relay peaks of this spin system.

impossible. The low dispersion of the resonances of these side chains about the free-chain values are presumably a consequence of their hydrophilic character. Further, we were not able to explore the un-ionized state of these side chains since the protein is unstable below pH 5. Assignment of these acidic residues was based largely on sequence-specific connectivities to neighboring amino acids with well-defined spin systems.

It is interesting to note that the trypsin-solubilized heme binding domain of cytochrome b_5 does not include any residues containing sulfur. Despite this lack of cysteine cross-links, the protein exhibits a remarkable degree of thermal stability. Thus, NMR spectra could be collected at relatively high temperatures, yielding correspondingly narrow lines.

Sequence-Specific Resonance Assignments. For regions of regular secondary structure, interresidue connectivity can be established with H_2O NOESY spectra. The short interresidue distances that can be detected in H_2O NOESY spectra are the C^{α}, C^{β}, and amide protons of one residue and the amide protons of the next residue (Wüthrich et al., 1982). These short distances will be referred to as $d_{\alpha N}$, $d_{\beta N}$, and d_{NN}, respectively. Interresidue NOESY connectivities that define the sequence-specific assignments are illustrated schematically in Figures 5 and 7. Cytochrome b_5 is 60% helical and contains a five-stranded β-sheet which constitutes 30% of the residues present. A detailed discussion of NOESY connectivities which define each region of secondary structure follows.

(A) β-Sheet Region. The pattern of a weak $C^{\alpha}H_i$–NH_i cross peak followed by a strong $C^{\alpha}H_i$–NH_{i+1} cross peak is expected for a β-structure. This pattern was often difficult to trace due to peak overlap and anomalous chemical shifts. While this problem existed for each species variant to some degree, the pattern was clearly traceable through a comparison of the connectivity paths. For example, for the β-strand extending from Thr-21 to Tyr-30, overlap between such cross peaks was resolved by examining the NOESY spectra of both the bovine (Figure 6a) and porcine (Figure 6b) proteins. Substantial shifts not only occur at the site of variation [e.g., Tyr-27 (bovine) → His-27 (porcine)] but extend in both directions

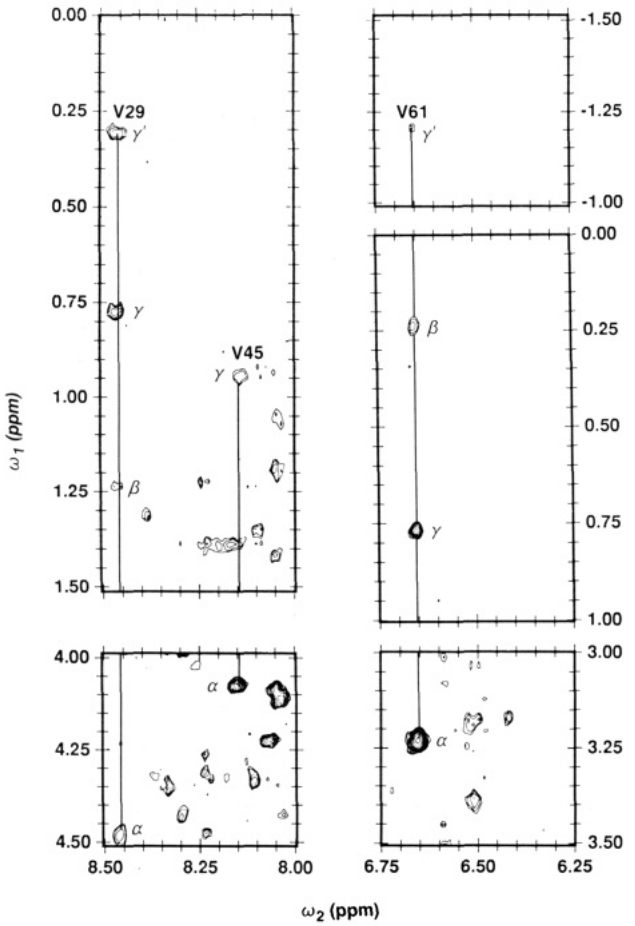

FIGURE 4: Contour plots of sections of the amide region of the HOHAHA spectrum of bovine cytochrome b_5 recorded at 40 °C in H_2O. The regions shown contain the direct $C^{\alpha}H$–NH cross peaks for three of the four valines and the relay peaks corresponding to NH–$C^{\beta}H$ and NH–$C^{\gamma}H$ or $C^{\gamma'}H$ relays.

along the primary sequence, resulting in an altered overlap pattern that would be difficult to assign in either spectrum alone. For example, in the bovine spectrum, the fingerprint peak and the $C^{\alpha}H_i$ to NH_{i+1} peaks often severely overlap (e.g., for Trp-22, Lys-28, and Tyr-27) while in the porcine spectrum these peaks are clearly resolved.

Figure 7 contains a schematic of the β-sheet region illustrating all sequential and nonsequential interresidue NOEs that define this element of secondary structure. Sequential assignments reported here for the β-sheet region are largely in agreement with a recent publication of this region for the trypsin-solubilized bovine liver microsomal cytochrome b_5 (Veitch et al., 1988). As indicated in Figure 7, a number of interchain NOEs also clearly support the β-sheet structure shown. Also shown in Figure 7 is one of the closed-loop NOE patterns used in the main chain directed strategy (Di Stefano & Wand, 1987) to establish the existence of antiparallel β-strand regions. The fidelity of this pattern across the triple-stranded antiparallel β-sheet region is quite low. However, this is perhaps consistent with the β-sheet structure determined by X-ray diffraction in that there are a number of deviations from a regular antiparallel structure (Mathews et al., 1979), see below.

(*B*) *Helices.* The characteristically short distances in helices, d_{NN} and $d_{\beta N}$, did not lead to unique NOE connectivities because of extensive resonance overlap. As noted earlier, deconvolution of aligned amide resonances was accomplished by examining their temperature-dependent variation and by examining the differences between species. Figure 8 contains

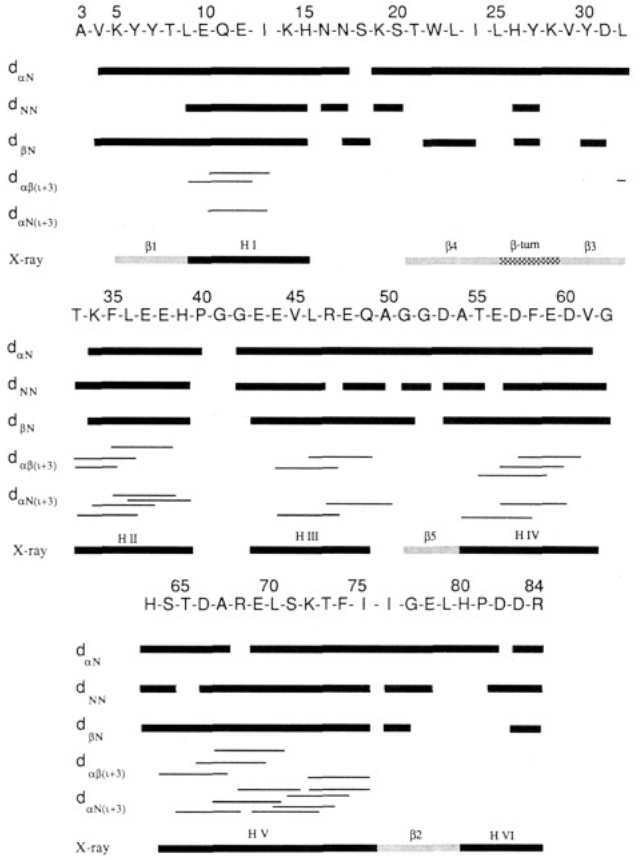

FIGURE 5: Summary of sequence-specific connectivities for cytochrome b_5. The $d_{\alpha\delta}$ connectivities for the two prolines are indicated by $d_{\alpha N}$ connectivities on the diagram. Midrange connectivities for the helical segments are also shown. The secondary structural elements found in the crystal structure are also indicated; helical domains are indicated by solid lines, portions of the β-sheet are indicated by shaded lines, and the tight β-turn within the β-sheet is indicated by a cross-hatched segment. Secondary structural domains are given the labels used by Mathews el al. (1979).

the NH_i to NH_{i+1} connectivity pattern for helix V (Thr-65 to Ile-75), which is the longest continuous helical segment in cytochrome b_5. More than 50% of the midrange connectivities (e.g., $C^{\alpha}H_i$ to NH_{i+3} or $C^{\alpha}H_i$ to $C^{\beta}H_{i+3}$) characteristic of helical structure were found, largely confirming the assignment of the helical segments (see Figure 5).

Another useful technique for assignments in helices was the main chain directed method (Englander & Wand, 1987; Di Stefano & Wand, 1988). Approximately 78% of the expected closed-loop patterns of NOEs between pairs of amino acids within the helical regions of the protein were observed. However, it should be noted that this pattern consists of only three NOESY peaks and only two are interresidue NOEs. Breaks in the continuity of this pattern of NOEs occurred principally due to missing or ambiguous $C^{\beta}H_i$–NH_{i+1} cross peaks or due to aligned amide resonances that result in NH_i–NH_{i+1} cross peaks either directly on the diagonal or too close to be resolved.

CORMA. Calculations of relative NOESY peak intensities from the X-ray coordinates were remarkably helpful throughout the assignment procedure. In several cases, we observed unexpectedly strong or weak NOESY cross-peak intensities on the basis of ideal secondary structure geometry. In all these cases, the intensities calculated with the CORMA procedure and the actual interatomic distances quantitatively matched the observations. For example, the intense d_{NN} connectivities between Gly-51 and Gly-52, within the β5 strand, and between Ile-76 and Gly-77 within the β2 strand,

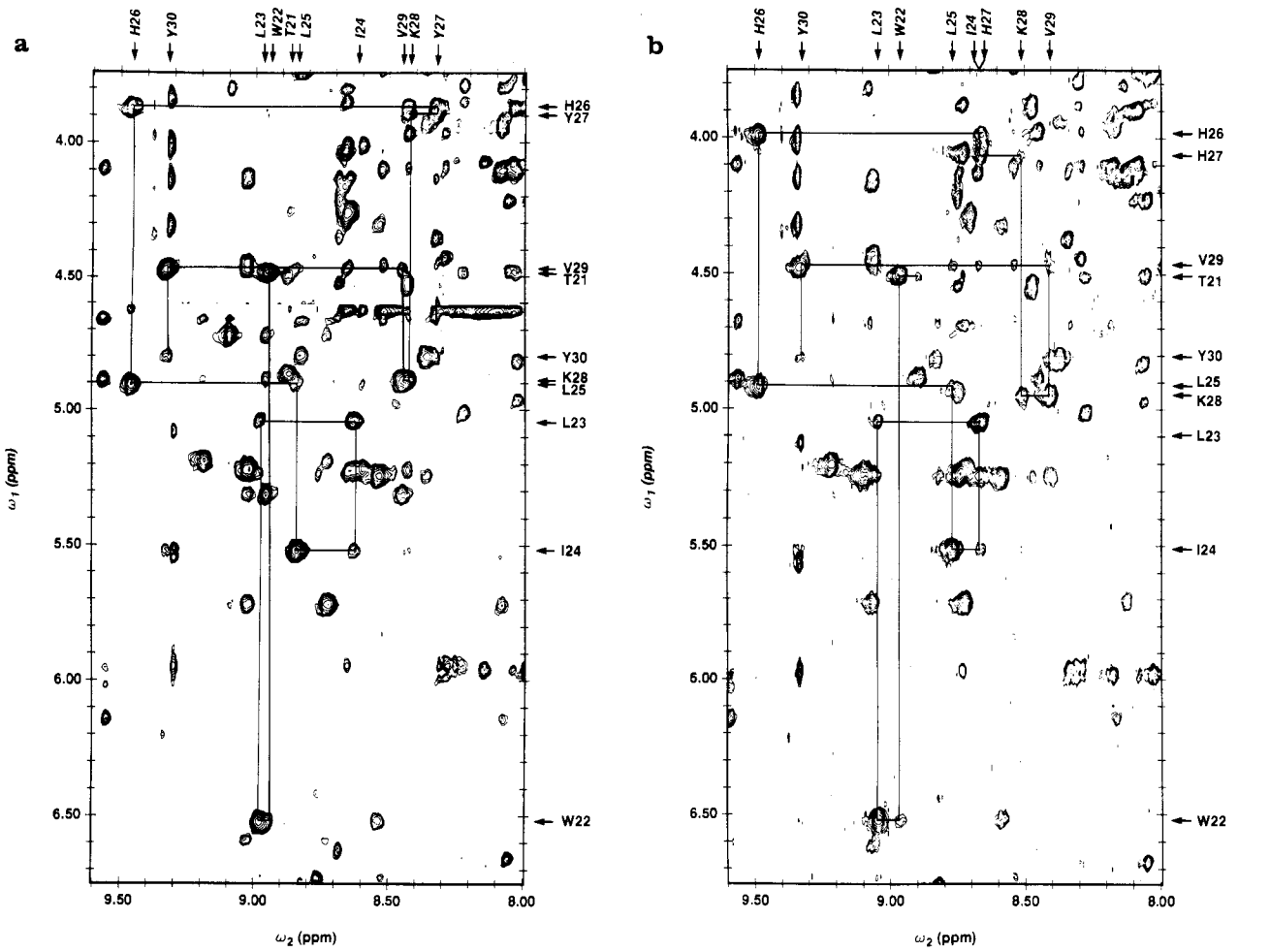

FIGURE 6: Portion of the NOESY spectrum of (a) bovine and (b) porcine cytochrome b_5 in H_2O at 40 °C and pH 7.0 showing the $d_{\alpha N}$ connectivities for residues 21–30.

are consistent with the crystal structure distances. For regions of regular secondary structure, calculation of sequential, midrange, and even long-range NOESY peak intensities was remarkably accurate. Table II contains a list of selected peak intensity ratios for the $\beta3$–$\beta4$ strands and for helix I. Considering the fact that a 10% difference in distances yields nearly a factor of 2 difference in NOE peak intensity due to the sixth power dependence, the agreement is actually quite good.

Ring-Current Calculations. It has been claimed that the heme ring-current shifts create unrecognizable cross-peak patterns and disrupt the sequential assignment procedure (Englander & Wand, 1987). See, for example, resonance assignments for Val-61 and Gly-41 in Table I. Fortunately, it was possible to calculate by the method of Johnson and Bovey (1958) the shifts in proton resonances from all the aromatic rings including the heme and to locate highly perturbed resonances. Ring-current intensity factors were those of Perkins and Dwek (1980).

Table III contains a comparison of calculated ring-current shifts and observed shifts from free-chain resonance positions (Bundi & Wüthrich, 1979) for a set of 86 protons in cytochrome b_5 for which calculated or observed values exceed at least 0.2 ppm. Calculated ring-current shifts for the methyl resonances are in good agreement with previous work (Keller & Wüthrich, 1980) (see Table III). The magnitude of the shifts observed is significantly larger than those observed in non-heme proteins. For example, in BPTI only two proton resonances have been reported with aromatic ring-current shifts larger than 0.2 ppm (Perkins & Wüthrich, 1979). Although a substantial number of shifts greater than 0.3 ppm have been reported in lysozyme due to the six tryptophan residues (Perkins & Dwek, 1980), few are as large as those observed in cytochrome b_5 (see, for example, the Gly-41 C^α proton shift in Table III). It is interesting to note that the large shifts

Table II: Comparison of Calculated and Experimentally Observed NOESY Peak Ratios

residue	calcd[a]	obsd[b]
$\beta3$–$\beta4$ Strand ($C^\alpha H_i$–NH_i/$C^\alpha H_i$–NH_{i+1})		
Trp-22	3.24	2.17
Leu-23	3.04	3.30
Ile-24	4.13	7.38
Leu-25	5.43	1.70
His-26	0.54	1.81
Tyr-27	5.92	3.98
Lys-28	4.90	*c*
Val-29	7.00	4.27
Tyr-30	7.32	6.85
Asp-31	5.77	5.32
Helix I (NH_i–NH_{i+1}/$C^\alpha H_i$–NH_{i+1})		
Leu-9	4.30	2.46
Glu-10	3.70	2.43
Gln-11	1.53	6.88
Ile-12	3.88	4.85
Glu-13	3.09	3.27
Lys-14	3.90	*d*

[a] Calculated values were determined from ratios of peak intensities obtained from a CORMA analysis using the crystal structure coordinates. [b] Ratios of integrated peak intensities from NOESY spectra. [c] Partial overlap of Lys-28 and Glu-48 fingerprint peaks made an accurate determination of the intensity of the Lys-28 fingerprint difficult. [d] Partial overlap of Thr-73 and Lys-14 fingerprint peaks made an accurate determination of the Lys-14 fingerprint peak difficult.

Table III: Comparison of Calculated Ring-Current Shifts and Experimentally Observed Shifts from Free-Chain Values

proton	calcd[a]	obsd[b]	proton	calcd[a]	obsd[b]
Ala-54C$^{\beta}$H	0.41	0.38	Ile-76C$^{\delta}$H	−2.68	−1.90
Ala-67C$^{\beta}$H[c]	−0.49	−0.18	Leu-23C$^{\alpha}$H	0.23	0.67
Asp-31C$^{\beta}$H	−0.04	0.26 (0.34)[d]	Leu-23C$^{\beta}$H	0.28	0.59
Asp-31C$^{\beta'}$H	−0.64	−0.88 (−0.79)	Leu-23C$^{\gamma}$H	0.30	0.21
Asp-57C$^{\beta}$H	−0.11	−0.29 (−0.20)	Leu-23C$^{\delta}$H	0.32	0.08 (0.12)
Asp-57C$^{\beta'}$H	−0.12	−0.09 (0.00)	Leu-23C$^{\delta'}$H	0.35	0.12 (0.16)
Asp-66C$^{\beta}$H	0.21	0.08[e]	Leu-25C$^{\delta}$H[c]	−0.77	−1.39 (−1.35)
Glu-37C$^{\alpha}$H	−0.43	−0.51	Leu-25C$^{\delta'}$H[c]	0.06	−0.30 (−0.26)
Glu-37C$^{\beta}$H	−0.24	−0.37 (−0.25)	Leu-36C$^{\alpha}$H	−0.68	−1.43
Glu-37C$^{\beta'}$H	−0.22	−0.21 (−0.09)	Leu-36C$^{\beta}$H	−0.30	−0.10
Glu-37C$^{\gamma}$H	−0.22	−0.23	Leu-36C$^{\delta}$H	−0.34	−0.45 (−0.41)
Glu-38C$^{\alpha}$H	−0.36	−0.30	Leu-36C$^{\delta'}$H	−0.14	−0.20 (−0.16)
Glu-38C$^{\beta}$H	−0.10	−0.03 (0.09)	Leu-46C$^{\beta}$H	−0.40	−0.21
Glu-38C$^{\beta'}$H	−0.30	−0.51 (−0.39)	Leu-46C$^{\beta'}$H	−0.60	−1.09
GluH43C$^{\alpha}$H	−0.74	−0.73	Leu-46C$^{\gamma}$H	−1.75	−1.45
Glu-43C$^{\beta}$H	−0.36	−0.43	Leu-46C$^{\delta}$H[d]	−1.38	−1.64 (−1.60)
Glu-43C$^{\beta'}$H	−0.47	−0.46 (−0.34)	Leu-46C$^{\delta'}$H[d]	−1.48	−1.70 (−1.66)
Glu-43C$^{\gamma}$H	−0.34	−0.43 (−0.40)	Leu-70C$^{\beta}$H	0.69	0.99
Glu-59C$^{\alpha}$H	−0.59	−0.51	Leu-70C$^{\beta'}$H	0.46	0.45
Glu-59C$^{\beta}$H	−0.21	−0.19[e]	Leu-70C$^{\gamma}$H	0.46	0.23
Phe-58C$^{\alpha}$H	−1.26	−0.81	Leu-70C$^{\delta}$H[c]	0.23	−0.13 (−0.09)
Gly-41C$^{\alpha}$H	−3.16	−3.65	Leu-70C$^{\delta'}$H[c]	0.72	0.25 (0.29)
Gly-41C$^{\alpha'}$H	−0.52	−0.64	Lys-5C$^{\alpha}$H	−0.27	−0.27
Gly-42C$^{\alpha}$H	−0.64	−0.04	Lys-5C$^{\beta}$H	−0.20	−0.17
Gly-42C$^{\alpha'}$H	−0.76	−0.64	Lys-14C$^{\beta}$H	−0.23	−0.23 (−0.14)
Gly-62C$^{\alpha}$H	−0.62	−0.59	Lys-14C$^{\beta'}$H	−0.29	−0.38 (−0.29)
Gly-62C$^{\alpha'}$H	−0.82	−0.81	Pro-40C$^{\alpha}$H	−0.53	−0.88
His-15C$^{\alpha}$H	−0.52	−0.51	Pro-40C$^{\delta}$H	−0.68	0.06
His-15C$^{\beta}$H	−1.38	−1.19 (−1.13)	Pro-40C$^{\delta'}$H	−2.52	−2.43
His-15C$^{\beta'}$H	−0.49	−0.73 (−0.67)	Pro-81C$^{\delta}$H	−0.82	−0.77
His-39C$^{\alpha}$H	−1.18	−2.19	Thr-55C$^{\gamma}$H[c]	−0.78	−0.83
His-39C$^{\beta}$H	−1.84	−2.42 (−2.39)	Thr-73C$^{\beta}$H	−1.30	−0.45
His-39C$^{\beta'}$H	−2.82	−2.78 (−2.72)	Thr-73C$^{\gamma}$H	−0.72	−0.14
His-63C$^{\alpha}$H	−2.10	−2.06	Val-4C$^{\alpha}$H	−0.20	−0.30
His-63C$^{\beta}$H	−2.18	−2.16 (−2.10)	Val-4C$^{\beta}$H	−0.22	−0.51
His-63C$^{\beta'}$H	−2.79	−2.88 (−2.82)	Val-4C$^{\gamma}$H	−1.13	−0.59 (−0.56)
Ile-75C$^{\alpha}$H	−0.62	−0.51	Val-4C$^{\gamma'}$H	−0.12	−0.33 (−0.30)
Ile-75C$^{\beta}$H	−0.19	−0.33	Val-45C$^{\gamma}$H[c]	−0.72	−0.17 (−0.13)
Ile-76C$^{\alpha}$H	−0.17	0.43	Val-45C$^{\gamma'}$H[c]	0.68	0.06 (0.10)
Ile-76C$^{\beta}$H	−0.29	−0.02	Val-61C$^{\alpha}$H	−0.39	−0.96
Ile-76C$^{\gamma}$H	−0.96	−1.16 (−0.87)	Val-61C$^{\beta}$H[c]	−0.33	−1.90
Ile-76C$^{\gamma'}$H	−1.01	−1.36 (−1.07)	Val-61C$^{\gamma}$H[c]	0.03	−0.18 (−0.15)
Ile-76C$^{\gamma}$H$_3$	−0.30	−0.13	Val-61C$^{\gamma'}$H[c]	−2.04	−2.20 (−2.17)

[a] Calculated ring-current shifts as described under Materials and Methods. [b] Experimentally observed shifts are the assigned values for each proton in cytochrome b_5 minus the free-chain value for the particular proton in that specific amino acid. Free-chain values are resonance positions determined from studies of tetrapeptides in solution (Bundi & Wuthrich, 1979). [c] Calculated values for these protons have been reported previously and are in good agreement with the present results (Keller & Wuthrich, 1980). [d] Solutions of tetrapeptides often exhibit two distinct values for these individual protons; both values have been used in the calculations shown. [e] The value reported here is the assigned value minus the average of the proton resonances observed in the free chain.

predicted for the two axial histidine C$^{\alpha}$ and C$^{\beta}$ proton resonances are observed. However, it is not possible on the basis of ring-current calculations alone to make the sequence-specific assignment for these two residues. The differences between the calculated and observed values could reflect real differences between the solution structure and the single-crystal X-ray structure or simply reflect limitations in the semiclassical calculation for protons in very close proximity to an aromatic ring. Variations of as little as 0.2 Å can cause resonance shifts of up to 0.2 ppm for protons in close proximity to an aromatic ring (Perkins, 1982). It is interesting to note that the largest relative errors are associated with the largest magnitude shifts, which would argue in favor of the latter hypothesis. The relative root mean square deviation between calculated and observed shifts for the values reported in Table III is 35%.

Generally, ring-current calculations have been thought to be less accurate for amide, aromatic, and C$^{\alpha}$ proton resonances (Perkins, 1982). We have found this to be true for amide protons. In some cases (e.g., Ser-64 and His-26) the predicted shift for the amide proton resonance was in the opposite direction to the observed shift. More commonly, the observed shift had the correct sign but was much larger than predicted (e.g., most notable in this regard are Asp-82, Ile-75, Leu-46, Val-61, and Tyr-30). Thus presumably other effects, such as hydrogen bonding, dominate over ring shift effects in determining the chemical shift of amide protons.

Surprisingly, we have found that the calculation of C$^{\alpha}$ proton resonance shifts is reasonably accurate (Figure 9). The correlation between calculated shifts and observed shifts is reasonably high (i.e., a linear regression analysis yields a slope of 0.994 with an intercept of −0.08 and a squared correlation coefficient of 0.62). Despite the reasonably high correlation, there appear to be other factors which affect C$^{\alpha}$ proton resonance positions. Close examination of Figure 9 reveals systematic trends in the difference between calculated and observed shifts which appear to correlate with secondary structure.

Chemical Shifts Characteristic of Secondary Structure. It has been suggested that C$^{\alpha}$ proton chemical shifts vary with secondary structure (Szilagyi & Jardetzky, 1989). Our data support this suggestion. Observed C$^{\alpha}$ proton chemical shifts corrected for ring-current effects. From these corrected C$^{\alpha}$ proton chemical shifts the free chain values (Bundi & Wüthrich, 1979) were subtracted. We found that the C$^{\alpha}$

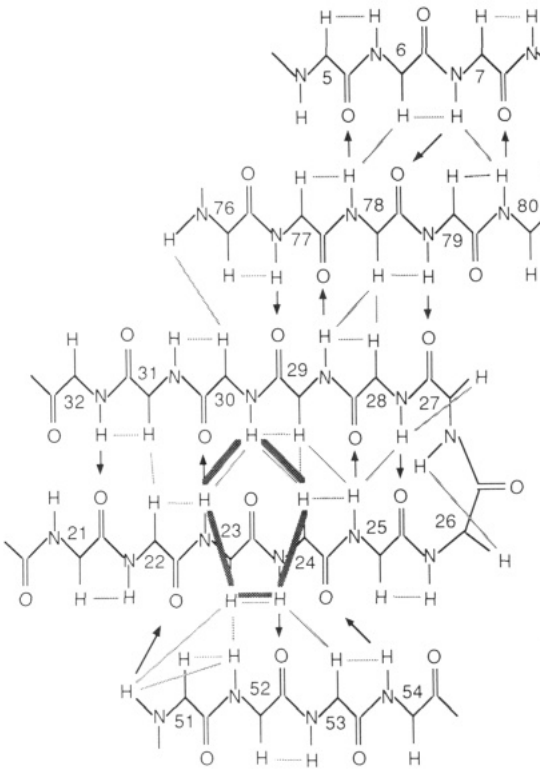

FIGURE 7: Schematic representation of the β-sheet region of cytochrome b_5. The hydrogen bonds found in the crystal structure (solid arrows) and the NOESY connectivities (shaded lines) determined from solution spectra of the bovine and porcine proteins recorded in H_2O and D_2O are illustrated. One closed loop pattern of intra- and interresidue NOESY connectivities characteristic of antiparallel β-sheet structure is also shown (heavy shaded lines).

proton resonances in helices were 0.31 ± 0.30 ppm less than the free-chain values and the resonances in the β-sheet were 0.39 ± 0.33 ppm greater than the free-chain values. We did not include the C^α proton resonance of Phe-58 because its C^α proton resonance difference of +0.45 ppm was an extreme outlier from the normal distribution observed for the other helical residues. Given this single exception, the differences between the means observed between α-helical C^α proton resonances and β-sheet C^α proton resonances were found to be statistically significant to within an 80% confidence interval. The statistical significance was evaluated on the basis of a Student's t test (i.e., $t = 1.34$ was greater that $t_{cr} = 1.29$ for 60 degrees of freedom), given two unequal populations with different variances (Glantz, 1981). Note that these shifts are in reasonable agreement in direction and magnitude with previously reported shifts associated with secondary structure (Szilagyi & Jardetzky, 1989). However, they report statistically significant trends for five amino acids and did not correct for ring-current effects. The lower statistical significance of our results is presumably due to a smaller number of data points.

Discussion

There are two areas that merit further consideration: our experience with various assignment strategies and a comparison of the secondary structure determined by NMR and X-ray experiments.

Sequence-Specific Resonance Assignment Strategy. The assignment of cytochrome b_5 was complicated for several reasons: (1) The protein exists in solution as an equilibrium mixture of two conformations that differ by the rotation of the heme about the α,γ-meso axis. (2) The heme is noncovalently bound, thus limiting the pH stability of the protein and requiring experiments at pH 7. (3) The large ring-current shifts from the heme made assignment of the side-chain spin systems difficult. (4) Cytochrome b_5 is a highly anionic protein and showed a small degree of chemical shift dispersion among the acidic side chains.

To overcome these problems, we were forced to modify the basic strategy established by Wüthrich and co-workers (Wüthrich, 1986) with additional computational methods and experiments. Specifically, we used the main-chain assignment procedures of Eads and Kuntz (1989) and Wand and Englander (Di Stefano & Wand, 1987; Englander & Wand, 1987), ring current calculations, and estimates of NOE intensities from the CORMA program. The latter two calculations were based on the atomic coordinates from the X-ray crystal structure. We also placed heavy reliance on spectra obtained at different temperatures and on the spectra obtained from three species variants. We discuss each of these topics in more detail, below.

The automated analysis of the main-chain resonances of cytochrome b_5 using the method of Eads rapidly yielded a set of 86 arbitrarily labeled spin systems. This technique worked well for the majority of the amino acids associated with the dominant form of the protein. However, it could not discriminate against some resonances associated with the minor-abundance form of the protein. Also, some of the spin systems of the dominant conformer were not identified due to missing fingerprint peaks, which we attribute to small $^3J_{N\alpha}$ couplings (Basus, 1989). At first glance, one might have drawn the erroneous conclusion that the elevated pH used in our experiments resulted in the rapid exchange of many amide protons, causing fingerprint peaks too broad to be observed. However, the intense C^α proton to amide proton NOESY cross peaks observed in these cases indicate that the absence of the COSY or HOHAHA peaks was due to a very small C^α proton amide proton coupling and not to exchange broadening. An examination of the ϕ angles determined in the crystal structure provides some support for this assertion. For example, Thr-55 and Leu-36 have ϕ angles of −37° and −40°, respectively. Calculating the magnitude of the C^α proton to amide proton coupling constant with the Karplus relation, calibrated with BPTI data (Pardi et al., 1984), one obtains $^3J_{N\alpha}$ couplings less than 2.5 Hz for these residues.

Potentially, the Eads program can yield sequence-specific resonance assignments in an automated manner, on the basis of searches through H_2O NOESY peak coordinate files for connectivities between the main-chain spin systems. For cytochrome b_5, it was not possible, on the basis of a single set of two-dimensional spectra for a single species at a single temperature, to determine a complete unambiguous set of sequential assignments. However, the result of this analysis was a rapid identification of the main-chain resonances of the majority of the spin systems present and a set of probable sequential connectivities between them that formed the framework for later work.

The main chain directed (MCD) assignment strategy was recently developed (Di Stefano & Wand, 1987; Englander & Wand, 1987) as an alternative to the Wüthrich approach when side-chain assignments are difficult. For cytochrome b_5, we found this technique to be most useful in the helical segments of the protein. Approximately 78% of the expected closed-loop patterns were observed. The technique was much less reliable for the β-sheet, presumably due to several significant distortions from regular secondary structure.

The use of ring-current calculations permitted several tentative sequential assignments that proved reliable. Similarly,

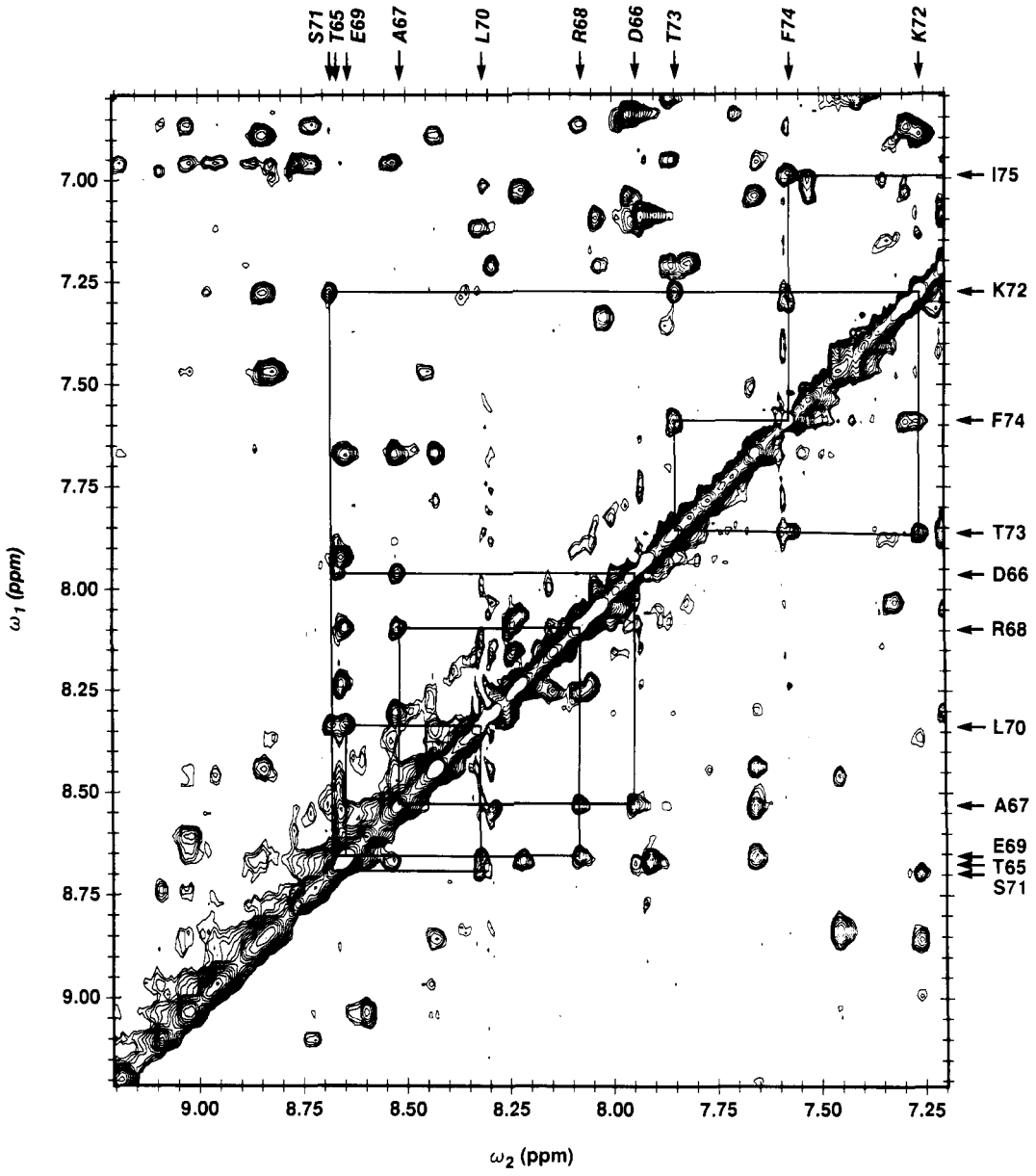

FIGURE 8: Contour plot of the amide–amide region of the NOESY spectrum in H_2O recorded at 40 °C, pH 7.0. Sequential connectivities between residues in helix V (T65 to I75) are indicated on the plot.

the NOE intensities calculated from CORMA allowed assignments in regions of the protein where the secondary structure was distorted from ideal geometry and confirmed assignments in regions of regular secondary structure. Finally, the species variants were indispensable for confirming sequential assignments.

A Comparison of Solution and Crystal Structures. Although a detailed discussion of specific differences in the solution and crystal structures is clearly not possible until a solution structure is calculated, certain qualitative similarities are apparent at the present level of analysis. In the discussion below, secondary structural elements will be referred to by the labels used by Mathews et al. (1979). The set of NOESY connectivities described below is indicated schematically in Figures 5 and 7.

For the β-sheet region, the presence of intense $d_{\alpha N}$ NOESY peaks from Val-4 to Thr-8 is in agreement with the β_1-strand (Lys 5 → Thr-8) indicated in the crystal structure. Although Val-4 is not considered part of this strand, the intense $d_{\alpha N}$ connectivity observed is predicted by the CORMA analysis. In the crystal structure the β_2-strand (Phe-74 → His-80) is somewhat distorted in the region around Ile-75; however, intense $d_{\alpha N}$ connectivities from Ile-75 to His-80 largely confirm the extended structure in solution. It is interesting to note that there is one significant difference in the antiparallel β3–β4 strand (Thr-21 → Leu-32) region indicated by the anomalously intense connectivity observed for His-26 to Tyr-27. This intense feature is suggestive that the β-turn (Leu-25 → Lys-28) is more like a type II turn in solution than the type I turn proposed by the X-ray analysis. Intense $d_{\alpha N}$ NOESY connectivities from Ala-50 to Ala-54 suggest that the β5 structure (Gln-51 → Ala-54) also exists in solution. The interstrand NOESY connectivities indicated schematically in Figure 7 largely confirm the existence of the five-stranded half β-barrel structure in solution.

The helical regions observed in the crystal structure are also largely confirmed in solution by the presence of both d_{NN} and $d_{\beta N}$ NOESY peaks. Thr-8 does not exhibit an observable d_{NN} connectivity to Leu-9 in helix I (Thr-8 → His-15). However, the intensity of this peak is predicted to be low by the CORMA analysis. Note that the distance between amide protons for Thr-8 to Leu-9 (i.e., 4.5 Å) determined from the crystal structure model is somewhat longer than that for subsequent pairs of amino acids in this helical segment. On the other

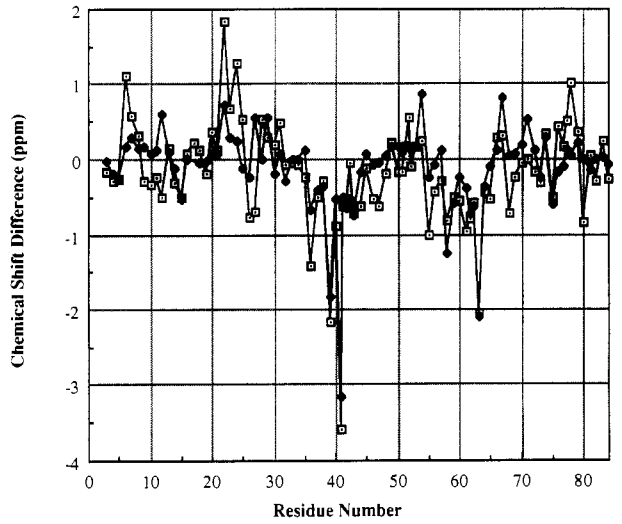

FIGURE 9: Comparison of predicted and experimental ring-current shifts for the C^{α} proton resonances of cytochrome b_5. Calculated ring-current shifts are indicated by the solid diamonds, and experimental values are indicated by the dotted squares. Experimental values of ring-current shifts were calculated by subtracting tabulated free-chain resonance values from C^{α} proton resonance assignments for cytochrome b_5.

hand, expected $d_{\beta N}$ connectivities between Thr-8 and Leu-9 are indicative of helical structure. All other d_{NN} and $d_{\beta N}$ connectivities from Leu-9 to His-15 suggest that helix I is present in solution. Except for the missing d_{NN} connectivity between Thr-33 and Lys-34, all d_{NN} and $d_{\beta N}$ connectivities from Leu-32 to His-39 are in agreement with the structure of helix II (Leu-32 → His-39) in the crystal structure. Amide proton to amide proton and $d_{\beta N}$ connectivities from Glu-43 to Ala-50 and from Ala-54 to Gly-62 are virtually all present as predicted by the helical segments III (Glu-43 → Gln-49) and IV (Ala-54 → Val-61) in the X-ray structure. Ser-64, the first residue of helix V (Ser-64 → Ile-75), does not exhibit a strong d_{NN} NOESY peak. This particular amide–amide NOESY cross peak is predicted to be unusually weak for a helical segment. Intense $d_{\beta N}$ cross peaks expected for a helical region are observed between Ser-64 and Thr-65. As predicted by the CORMA analysis, $d_{\beta N}$ connectivities for Phe-74 are not observed, but an intense d_{NN} cross peak is, confirming its position in the helix. Helix VI (His-80 → Arg-84) is a short, distorted helical segment with a proline in the middle. The presence of a strong $C^{\alpha}H_i$–$C^{\delta}H_{i+1}$ cross peak indicates that Pro-81 has a trans configuration. All expected $d_{\beta N}$ and d_{NN} connectivities from Asp-82 to Arg-84 are observed.

A number of high-resolution NMR studies (Reid et al., 1987; Veitch et al., 1988; McLachlan et al., 1988) indicate that the solution structure of cytochrome b_5 is a more dynamic entity than that found in the solid state. Previous studies have shown that a partial set of assigned aromatic residues are rapidly rotating at the temperatures examined (Veitch et al., 1988). We have confirmed their observations and in addition have found that all the tyrosines and phenylalanines in cytochrome b_5 are freely rotating. This is in contrast to more restricted aromatic side-chain mobilities observed in other proteins such as BPTI (Wüthrich & Wagner, 1978) and cytochrome *c* (Wand et al., 1989). McLachlan et al. (1988) have also shown that the 2-vinyl group of the heme flips between cis and trans configurations in solution while the cis configuration is the only form present in the crystal structure. It is interesting to speculate that the dynamic character of cytochrome b_5 in solution may be important in mediating its diverse range of physiological electron-transfer functions.

The assignments reported in this paper set the stage for a series of experiments directed at deducing structure–function relationships important to an understanding of the role of cytochrome b_5 as an electron-transfer protein. The recent assignment of the proton resonances of cytochrome *c* (Wand et al., 1989; Feng et al., 1989) makes a study of the complex formed between cytochrome *c* and cytochrome b_5 particularly attractive as a model system for the examination of interprotein electron transfer. Despite an array of optical (McLendon & Miller, 1985; McLendon et al., 1985), NMR (Eley & Moore, 1983; Burch et al., 1988), and theoretical (Salemme, 1976; Mauk & Mauk, 1986; Wendoloski et al., 1987) studies of the complex, no complete structural characterization of the complex has yet been possible. A structure of the complex formed between cytochrome b_5 and cytochrome *c* determined in solution based on two-dimensional NMR methods will no doubt yield important insights into structural features important to long-range biological electron transfer.

ACKNOWLEDGMENTS

We thank Dr. Jim Lipka for his efforts in the isolation and characterization of large quantities of the rabbit, pig, and calf liver trypsin-cleaved microsomal cytochrome b_5. We thank Dr. Vladimir Basus for assistance with data acquisition and for many useful discussions regarding the interpretation of two-dimensional NMR spectra. We thank Mark Day for improvements of the NMR data processing software. We are grateful to Dr. Brandan Borgias for assistance with the CORMA analysis. We are grateful to Dr. David Case for providing the ring-current shift calculation programs originally written by Dr. Keith Cross. We thank Dr. Charles Eads for assistance with his automated 2D NMR analysis programs. We are also grateful to the computer graphics laboratory at UCSF for the use of the facilities in the display and interpretation of the crystallographic data. The computer graphics laboratory at UCSF is supported by NIH Grant RR-01081 to Dr. Robert Langridge.

Registry No. Ferrocytochrome b_5, 9035-39-6.

REFERENCES

Abe, K., Kimura, S., Kizawa, R., Anan, F. K., & Sugita, Y. (1985) *J. Biochem. 97*, 1659–1688.

Altman, J., Lipka, J. J., Kuntz, I. D., & Waskell, L. (1989) *Biochemistry 28*, 7516–7523.

Basus, V. J. (1989) *Methods Enzymol. 177*, 132–149.

Basus, V. J., Billeter, M., Love, R. A., Stroud, R. M., & Kuntz, I. D. (1988) *Biochemistry 27*, 2763–2771.

Bax, A., & Davis, D. G. (1985) *J. Magn. Reson. 65*, 355–360.

Billeter, M., Braun, W., & Wüthrich, K. (1985) *J. Mol. Biol. 155*, 321–346.

Bundi, A., & Wüthrich, K. (1979) *Biopolymers 18*, 285–298.

Burch, A. M., Rigby, S. E. J., Funk, W., Macgillivray, R. T. A., Mauk, A. G., Mauk, M., & Moore, G. R. (1988) *Biochem. Soc. Trans. 16*, 844–845.

Canova-Davis, E., & Waskell, L. (1984) *J. Biol. Chem. 259*, 2541–2546.

Cantor, C. R., & Schimmel, P. R. (1980) in *Techniques for the Study of Biological Structure and Function*, p 461, W. H. Freeman, San Francisco.

Di Stefano, D. L., & Wand, A. J. (1987) *Biochemistry 26*, 7272–7281.

Eads, C. E., & Kuntz, I. D. (1989) *J. Magn. Reson. 82*, 467–482.

Eley, C. G. S., & Moore, G. R. (1983) *Biochem. J. 215*, 11–21.

Englander, S. W., & Wand, A. J. (1987) *Biochemistry 26*, 5953–5958.
Feng, Y., Roder, H., Englander, S. W., Wand, A. J., & Di Stefano, D. L. (1989) *Biochemistry 28*, 195–203.
Glantz, S. A. (1981) in *Primer of Biostatistics*, pp 63–93, MaGraw-Hill, New York.
Hegesh, E., Hegesh, J., & Kaftory, A. (1986) *N. Engl. J. Med. 314*, 757–761.
Hildebrandt, A., & Estabrook, R. W. (1971) *Arch. Biochem. Biophys. 143*, 66–79.
Hore, P. J. (1983) *J. Magn. Reson. 54*, 539–542.
Johnson, C. E., & Bovey, F. A. (1958) *J. Chem. Phys. 29*, 1012–1014.
Keepers, J. W., & James T. L. (1984) *J. Magn. Reson. 57*, 404–426.
Keller, R. M., & Wüthrich, K. (1980) *Biochim. Biophys. Acta 621*, 204–217.
Keller, R. M., Groudinsky, O., & Wüthrich, K. (1976) *Biochim. Biophys. Acta 427*, 497–511.
Kuwahara, S., & Omura, T. (1980) *Biochem. Biophys. Res. Commun. 96*, 1562–1568.
LaMar, G. N., Burns, P. D., Jackson, J. T., Smith, K. M., Langry, K. C., & Strittmatter, P. J. (1981) *J. Biol. Chem. 256*, 6075–6079.
Lederer, F., Ghrir, R., Guiard, B., Cortial, S., & Ito, A. (1983) *Eur. J. Biochem. 132*, 95–102.
Mathews, F. S., & Czerwinski, E. W. (1976) in *The Enzymes of Biological Membranes* (Martonosi, A., Ed.) Vol. 4, pp 143–197, Wiley, New York.
Mathews, F. S., Levine, M., & Argos, P. (1972) *J. Mol. Biol. 64*, 449–464.
Mathews, F. S., Czerwinski, E. W., & Argos, P. (1979) in *The Porphyrins* (Dolphin, D., Ed.) Vol. 7, pp 107–147, Academic Press, New York.
Mauk, M. R., & Mauk, A. G. (1986) *Biochemistry 25*, 7085–7091.
McLachlan, S. J., LaMar, G. N., Burns, P. D., Smith, K. M., & Langry K. C. (1986) *Biochim. Biophys. Acta 874*, 274–284.
McLachlan, S. J., LaMar, G. N., & Lee, K.-B. (1988) *Biochim. Biophys. Acta 957*, 430–445.
McLendon, G., & Miller, J. R. (1975) *J. Am. Chem. Soc. 107*, 7811–7816.
McLendon, G., Winkler, J., Nocera, D., Mauk, A. G., & Gray, H. B. (1985) *J. Am. Chem. Soc. 107*, 739–740.
Noshiro, M., Harada, N., & Omura, T. (1979) *Biochem. Biophys. Res. Commun. 91*, 207–213.
Oshino, N. (1978) *Pharmacol. Ther. 2*, 477–515.
Pardi, A., Billeter, M., & Wüthrich, K. (1984) *J. Mol. Biol. 180*, 741–751.
Pearson, G. A. (1977) *J. Magn. Reson. 27*, 265–272.
Perkins, S. J. (1982) *Biol. Magn. Reson. 4*, 193–336.
Perkins, S. J., & Wüthrich, K. (1979) *Biochim. Biophys. Acta 576*, 409–423.
Perkins, S. J., & Dwek, R. A. (1980) *Biochemistry 19*, 245–258.
Piantini, O. W., Sørensen, O. W., & Ernst, R. R. (1982) *J. Am. Chem. Soc. 104*, 6800–6801.
Pompon, D., & Coon, M. J. (1984) *J. Biol. Chem. 259*, 15377–15385.
Redfield, A. G., & Kunz, S. D. (1975) *J. Magn. Reson. 19*, 250–254.
Reid, L. S., & Mauk, A. G. (1982) *J. Am. Chem. Soc. 104*, 841–845.
Reid, L. S., Gray, H. B., Dalvit, C., Wright, P. E., & Saltman, P. (1987) *Biochemistry 26*, 7102–7107.
Salemme, F. R. (1976) *J. Mol. Biol. 102*, 563–568.
Shaka, A. J., & Freeman, R. (1983) *J. Magn. Reson. 51*, 169–173.
States, D. J., Haberkorn, R. A., & Ruben, D. J. (1982) *J. Magn. Reson. 48*, 286–292.
Strittmatter, P., & Velick, S. F. (1956) *J. Biol. Chem. 221*, 253–264.
Szilagyi, L., & Jardetzky, O. (1989) *J. Magn. Reson. 83*, 441–449.
Vatsis, K. P., Theoharides, A. D., Kupfer, D., & Coon, M. J. (1982) *J. Biol. Chem. 257*, 11221–11229.
Veitch, N. C., Concar, D. W., Williams, R. J. P., & Whitford, P. (1988) *FEBS Lett. 238*, 49–55.
Wand, A. J., Di Stefano, D. L., Feng, Y., Roder, H., & Englander, S. W. (1989) *Biochemistry 28*, 186–194.
Wendoloski, J. J., Mathews, J. B., Weber, P. C., & Salemme, F. R. (1987) *Science 238*, 794–797.
Wüthrich, K. (1986) *NMR of Proteins and Nucleic Acids*, Wiley, New York.
Wüthrich, K., & Wagner, G. (1978) *Trends Biochem. Sci. 3*, 227–230.
Wüthrich, K., Billeter, M., & Braun, W. (1984) *J. Mol. Biol. 180*, 715–740.